High- and low-temperature pyrolysis profiles describe volatile organic compound emissions from western US wildfire fuels

Kanako Sekimoto[1,2,3], Abigail Koss[1,2,4,*], Jessica B. Gilman[1], Vanessa Selimovic[5], Matthew M. Coggon[1,2], Kyle J. Zarzana[1,2], Bin Yuan[1,2,†], Brian M. Lerner[1,2,‡], Steven S. Brown[1,4], Carsten Warneke[1,2], Robert J. Yokelson[5], James M. Roberts[1], Joost de Gouw[1,2,4]

[1] NOAA Earth System Research Laboratory (ESRL), Chemical Sciences Division, Boulder, CO, USA

[2] Cooperative Institute for Research in Environmental Sciences, University of Colorado Boulder, Boulder, CO, USA

[3] Graduate School of Nanobioscience, Yokohama City University, Yokohama, Japan

[4] Department of Chemistry and Biochemistry, University of Colorado Boulder, Boulder, CO, USA

[5] Department of Chemistry, University of Montana, Missoula, MT, USA

[*] Now at Department of Civil & Environmental Engineering, Massachusetts Institute of Technology, Cambridge, MA, USA

[†] Now at Institute for Environment and Climate Research, Jinan University, Guangzhou, China

[‡] Now at Aerodyne Research, Inc., Billerica, MA, USA

Supporting Information

Contents

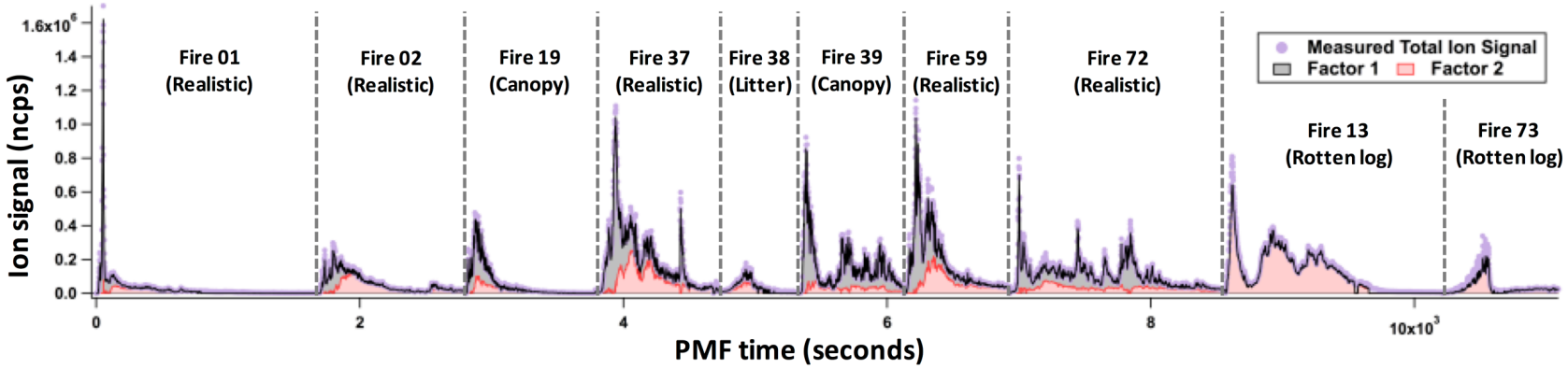

Figure S1. Time series of 2-factor PMF solution for Ponderosa pine dataset.

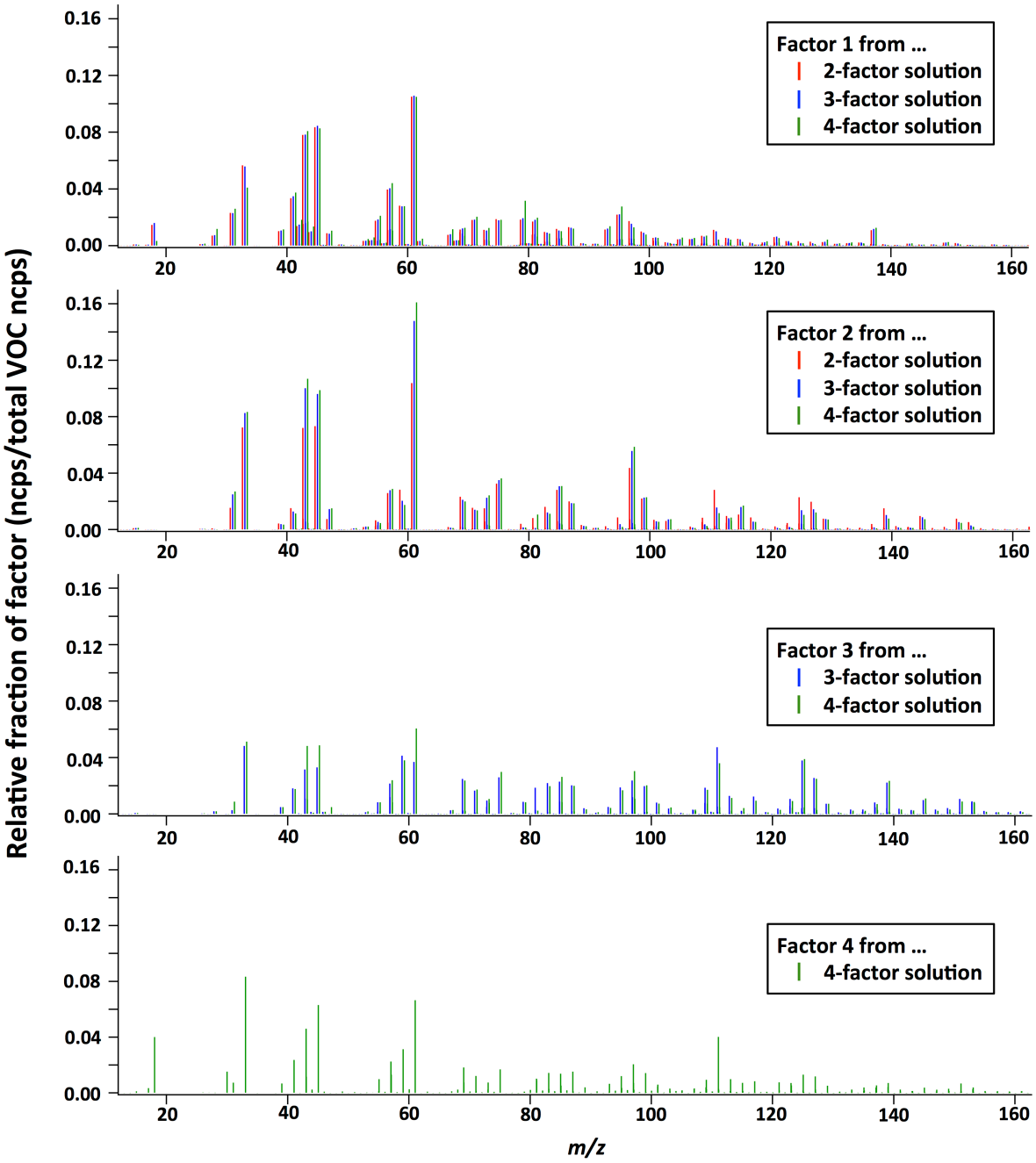

Figure S2. Comparison of mass spectra from 2-, 3-, and 4-factor PMF solutions. The two factors that account for most of the variability (Factor 1 and Factor 2) do not change substantially as the number of factors increases. The additional factors in the 3- and 4-factor solutions have similar mass spectra to Factor 1 and Factor 2.

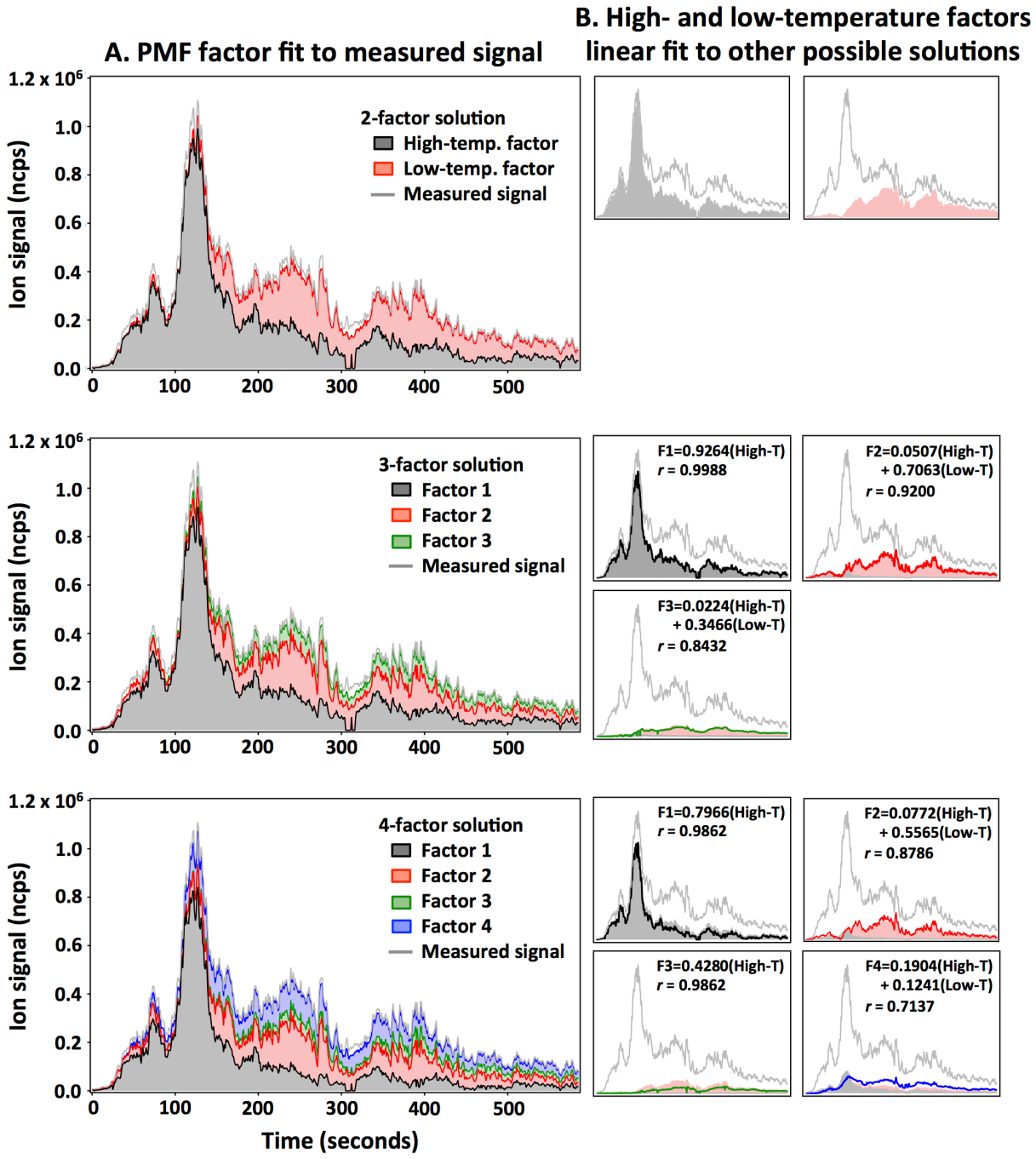

Figure S3. Comparison of time series from 2-, 3-, and 4-factor PMF solutions. The time series shown is the total instrument signal from a representative fire of Ponderosa pine (a part of Fire #37). The individual factors are from the PMF analysis of the extended time series (in which all ten fires of Ponderosa pine were concatenated). The left-side plots (A) show the stacked contributions of the factors, compared to the measured signal. The small plots on the right (B) show the time series of the individual factors (solid lines). The high- and low-temperature factors were fit to each factor in the 3- and 4-factor solutions. The best-fit was done using the extended time series. These best-fits are shown as the shaded areas in the right-side plots (B), and the best-fit equation and correlation coefficient are also provided.

Comparison of emission profile between each fuel and average (ncps/total VOC ncps)

(a) High-temperature pyrolysis factor

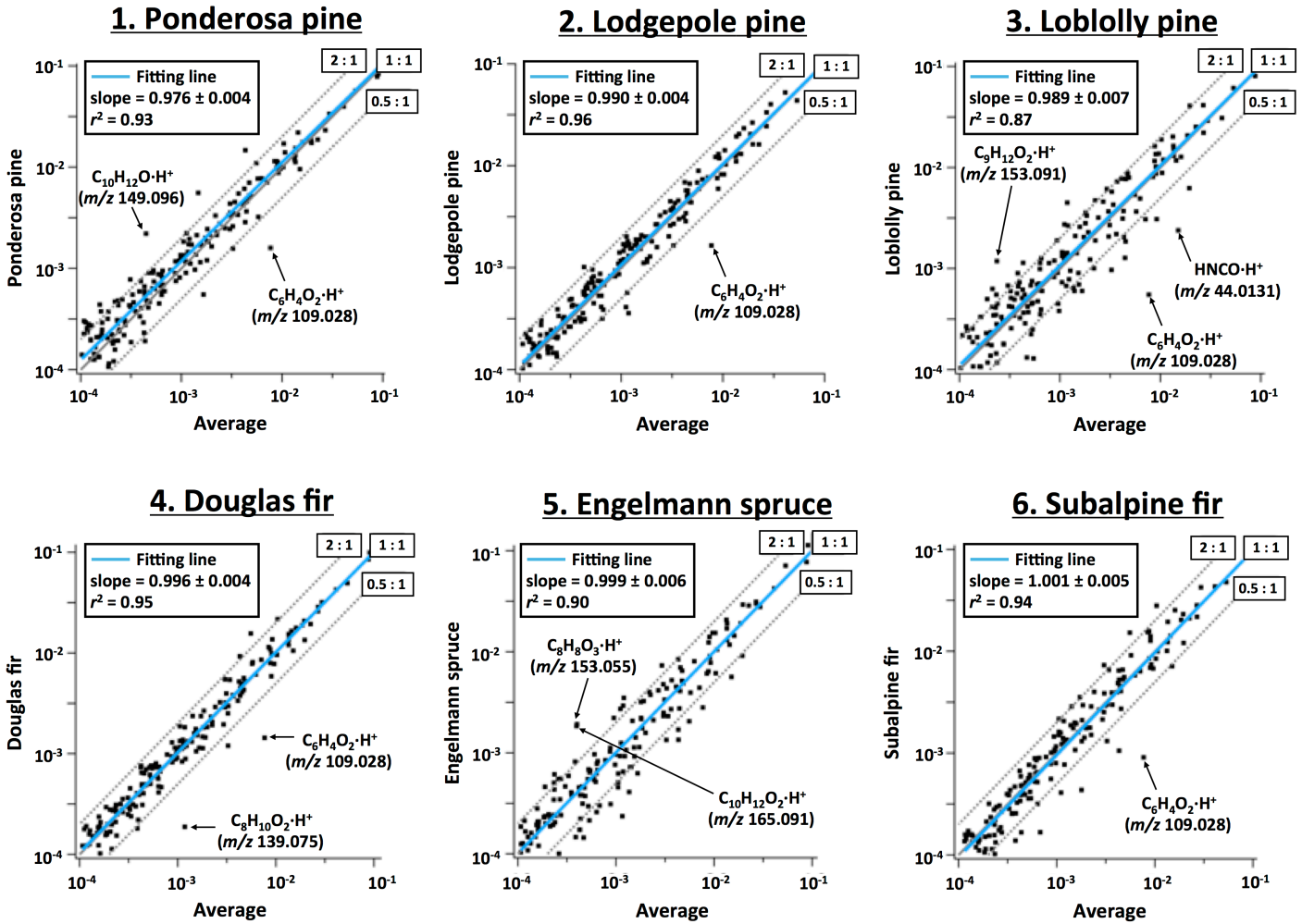

Figure S4. Comparison of (a) high- and (b) low-temperature pyrolysis VOC emission profiles (ncps/total VOC ncps) between each fuel and average of 15 different fuels shown in Figure 3. Data points in individual panels correspond to well-fitted 434 ion peaks. Slope and correlation coefficient (r2) are obtained using logarithmic fraction, i.e., log(ncps/total VOC ncps).

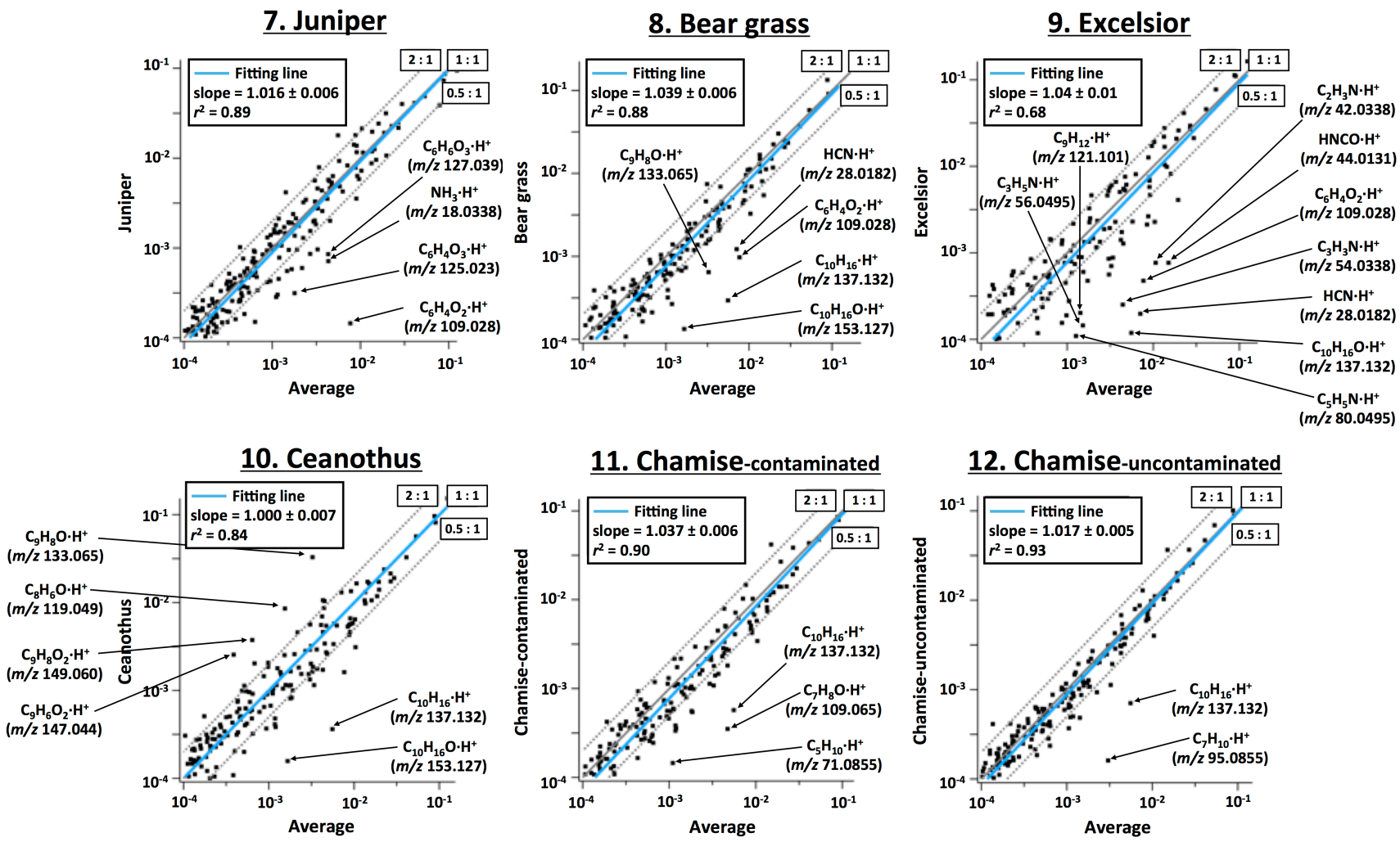

Figure S4. Continued.

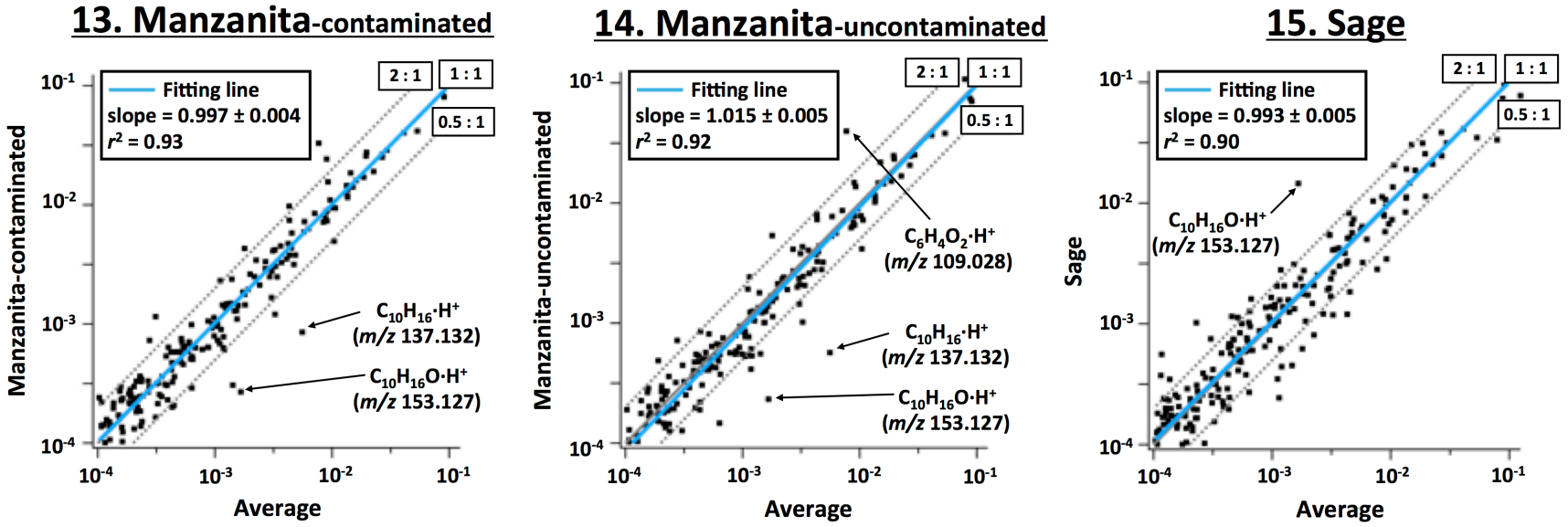

Figure S4. Continued.

(b) Low-temperature pyrolysis factor

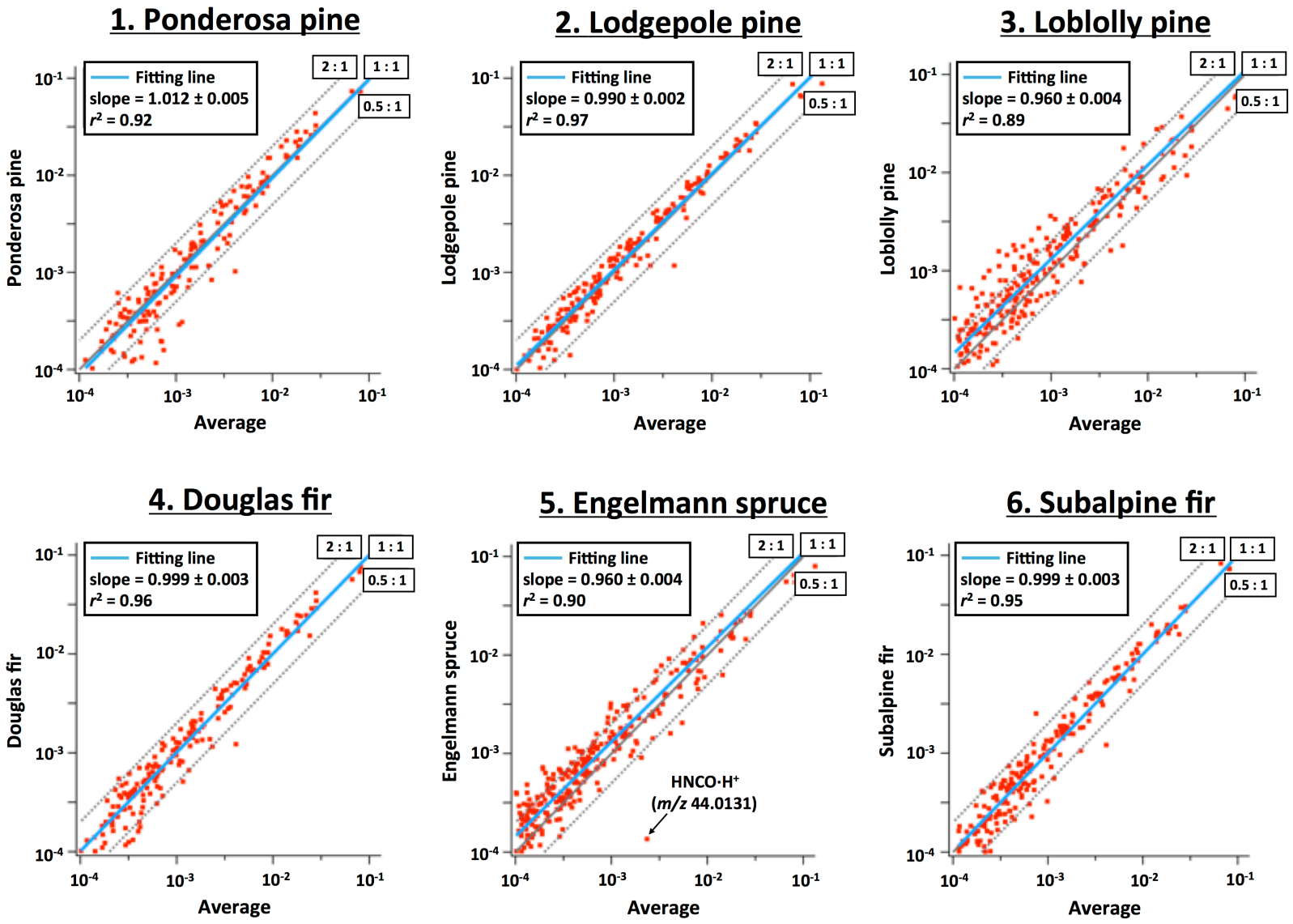

Figure S4. Continued.

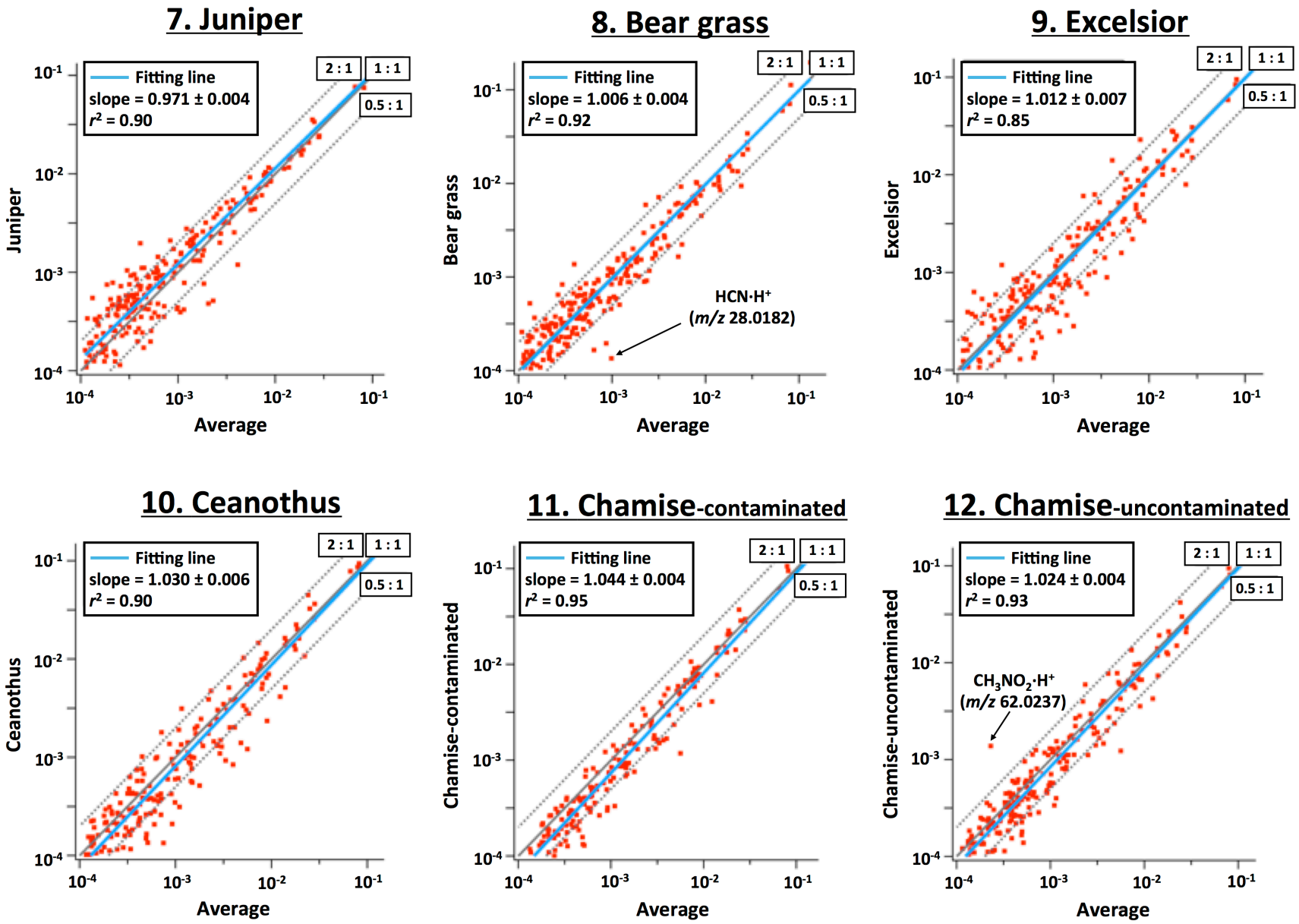

Figure S4. Continued.

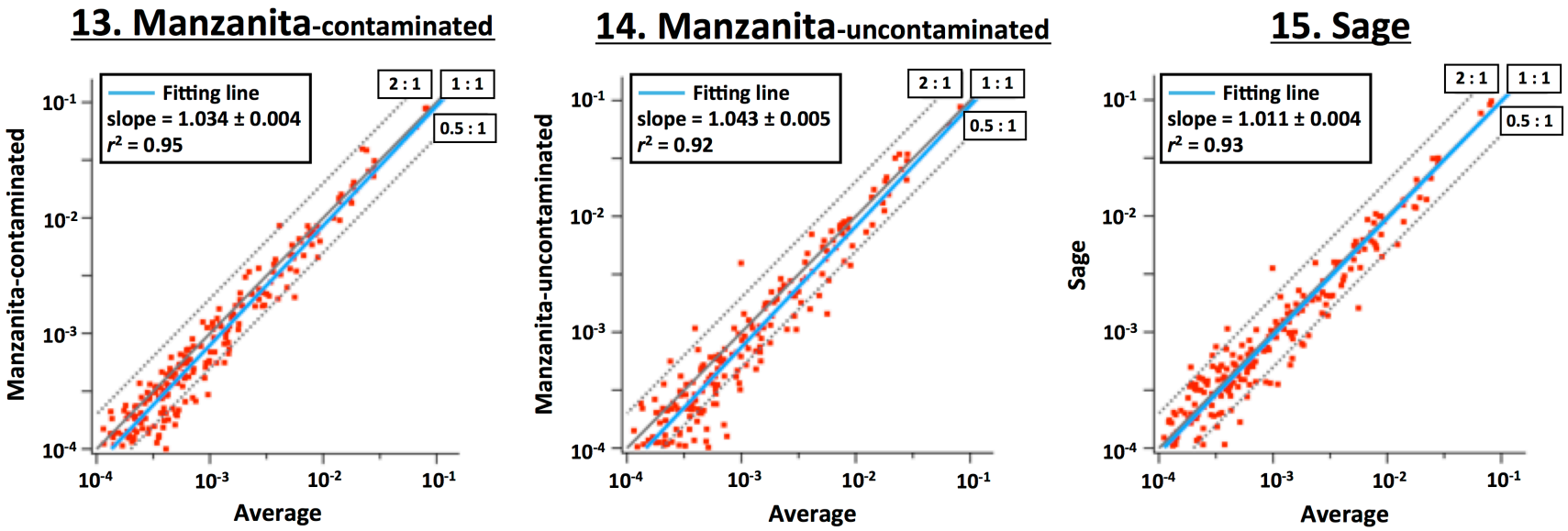

Figure S4. Continued.

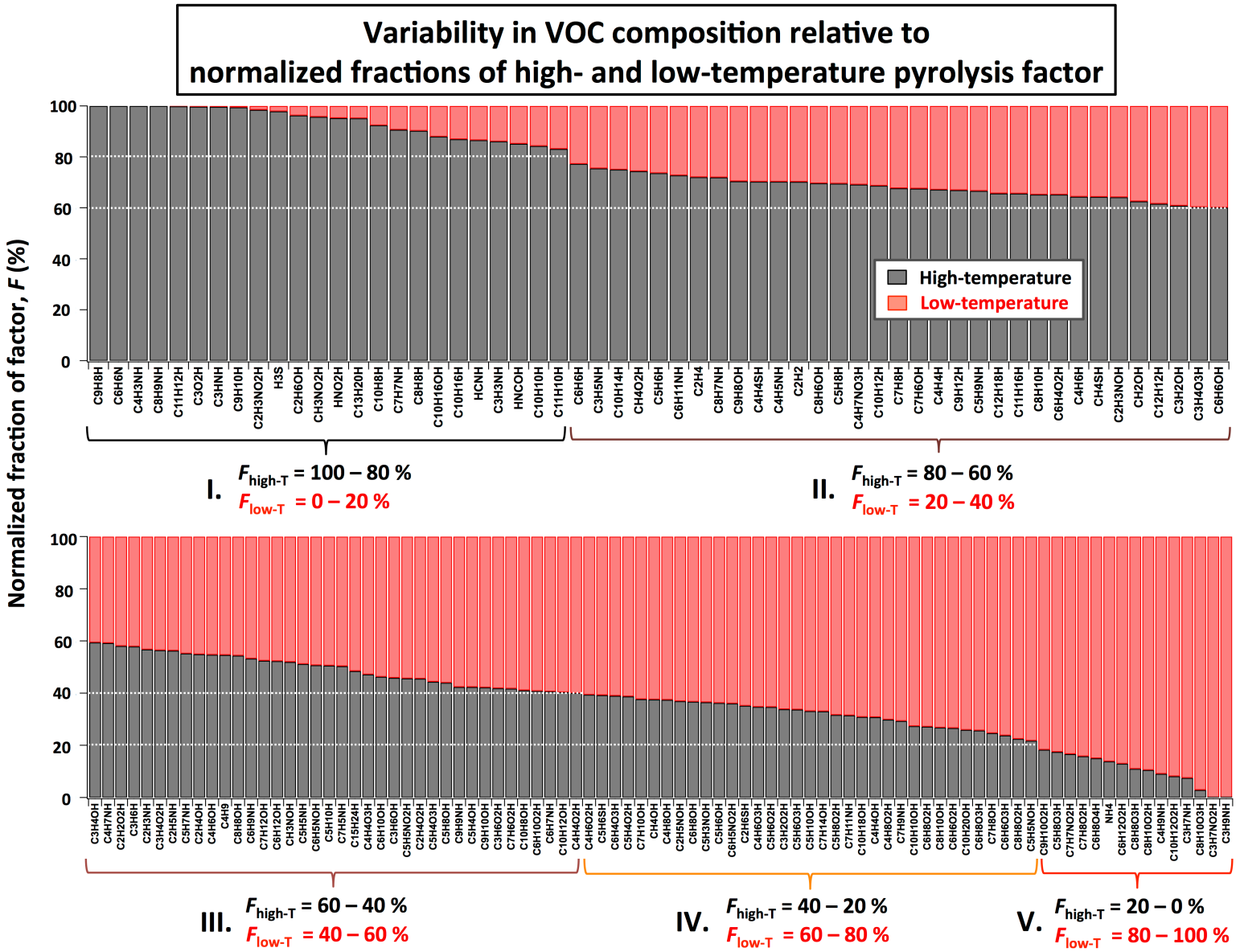

Figure S5. Variability in VOC composition relative to normalized fractions of the high- and low-temperature factors calculated from the average VOC profiles (Figure 3). The identified ion peaks were arranged in descending order of the normalized fraction of high-temperature factor.

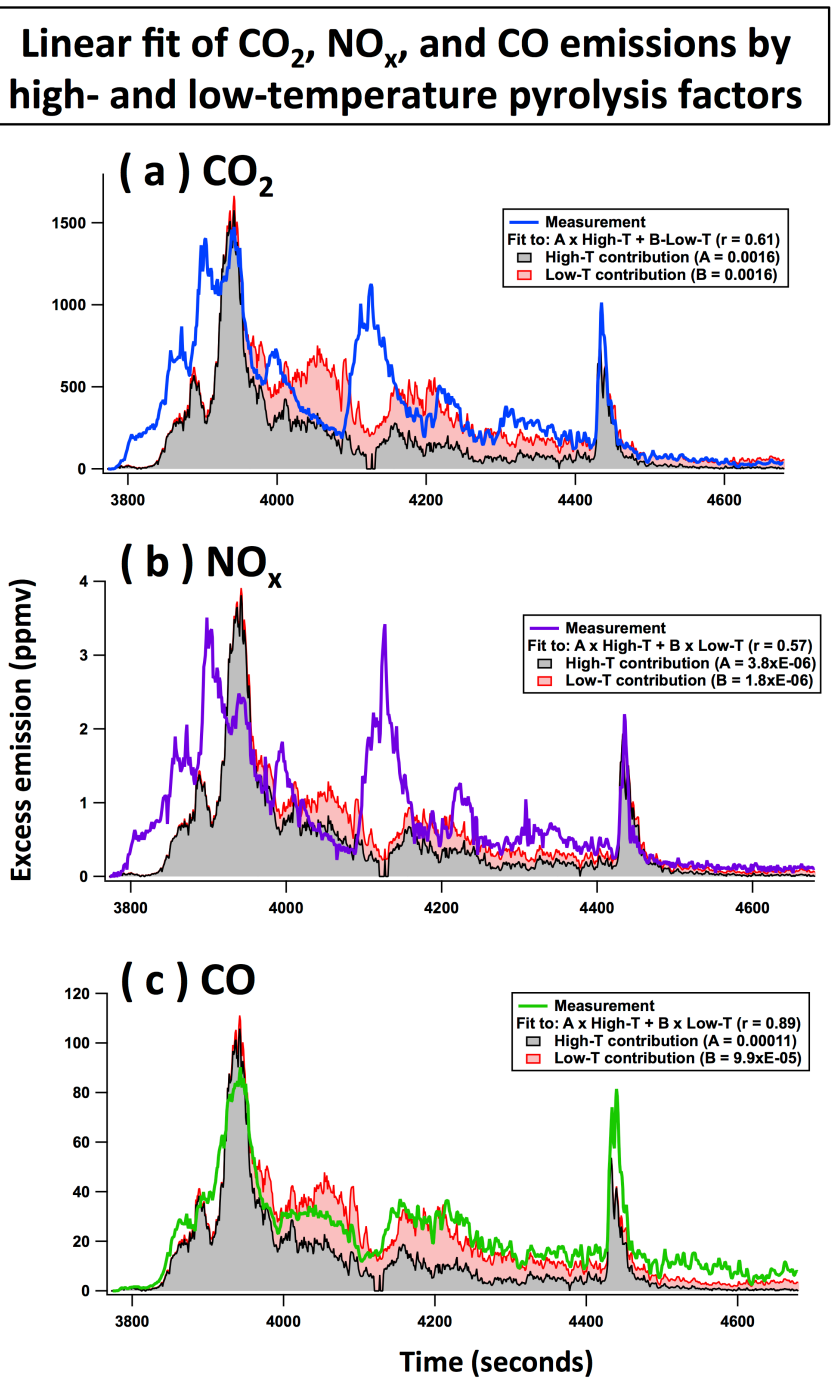

Figure S6. Linear fits of (a) CO_2, (b) NO_x, and (c) CO emissions (in ppmv) by the high- and low-temperature pyrolysis time series (in ncps) for Fire #37 (Ponderosa pine realistic mixture). Each plot shows the stacked contributions of the high- and low-temperature factors (shaded area), compared to the measured mixing ratios (solid line). The best-fit equation and correlation coefficient are also provided.

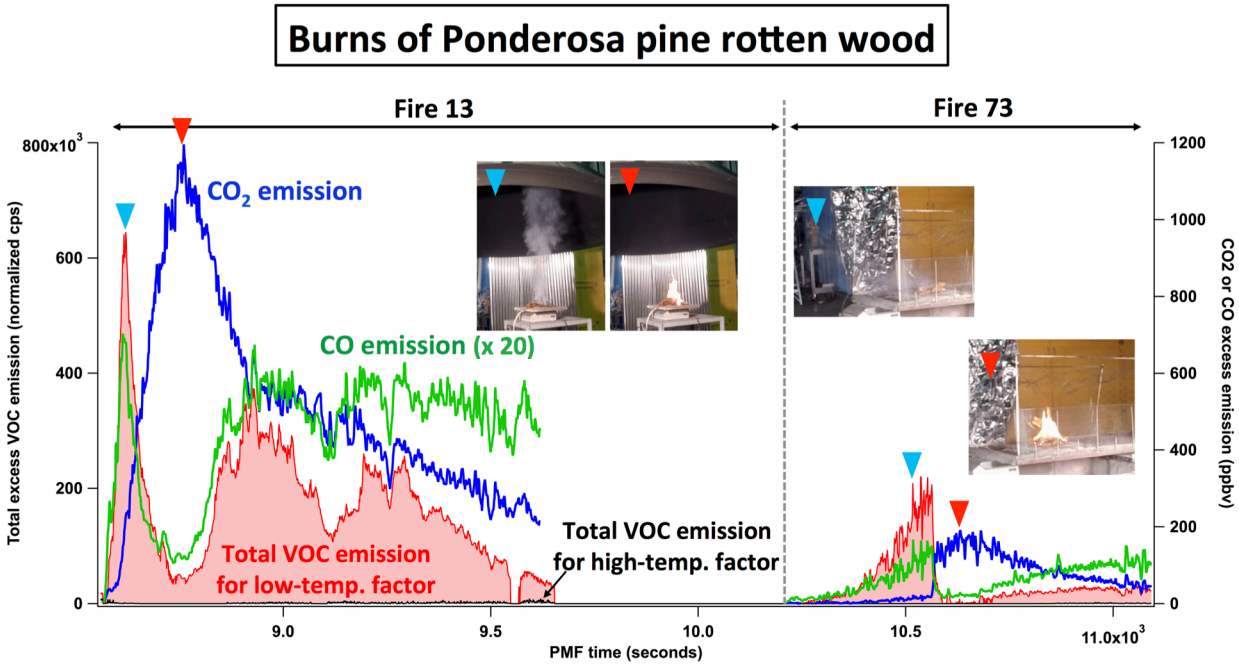

Figure S7. Results for burns of Ponderosa pine rotten wood (Fires #13 and #73).

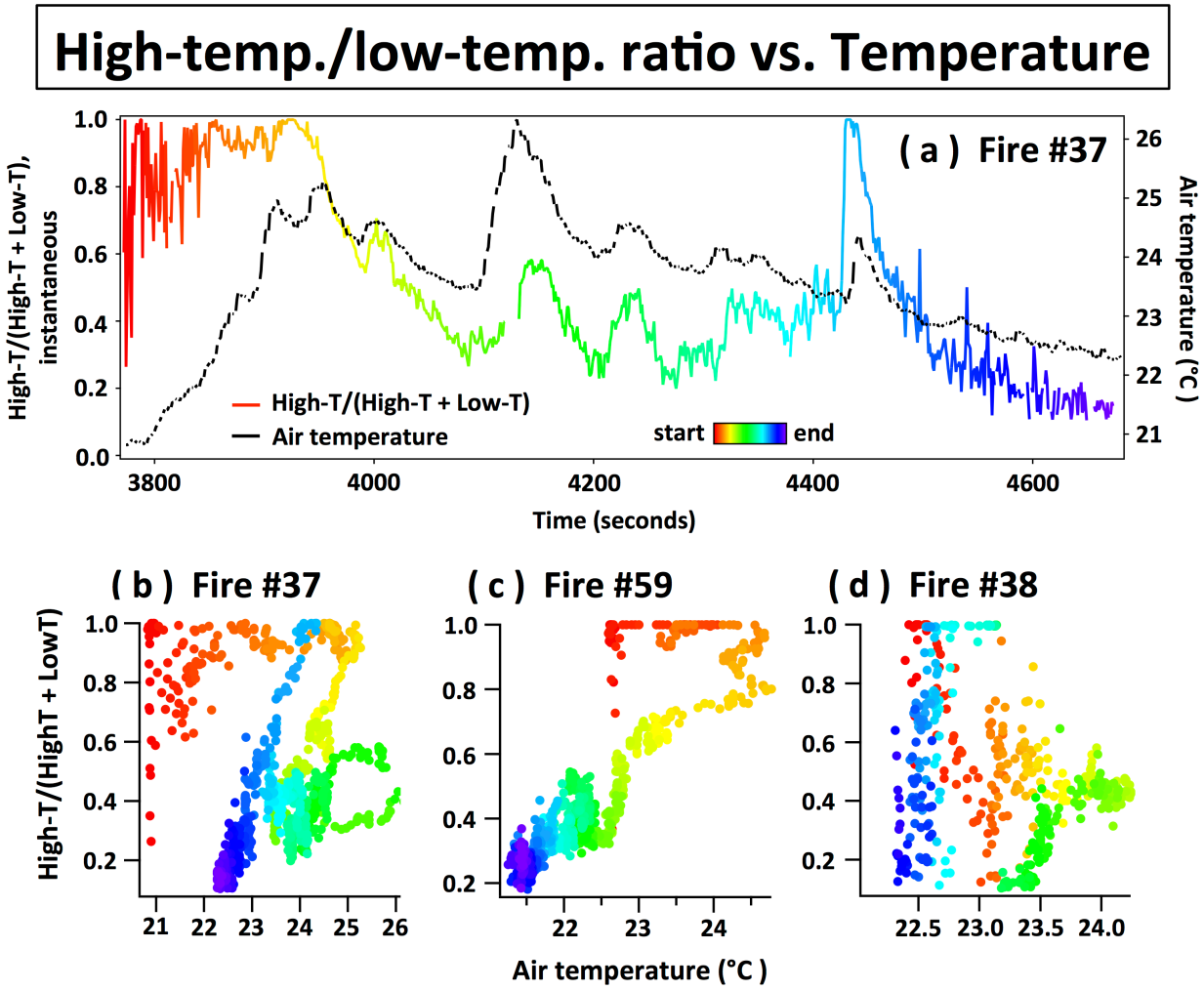

Figure S8. The comparison of contribution of high-temperature factor versus air temperature of the emissions measured at the sampling inlet of the PTR-ToF-MS. (a) Time series of Fire #37 (Ponderosa pine realistic mixture). (b)-(d) Scatter plots of instantaneous high-temperature contribution versus temperature for Fire #37, #59 (Ponderosa pine realistic mixture), and #38 (Ponderosa pine litter).

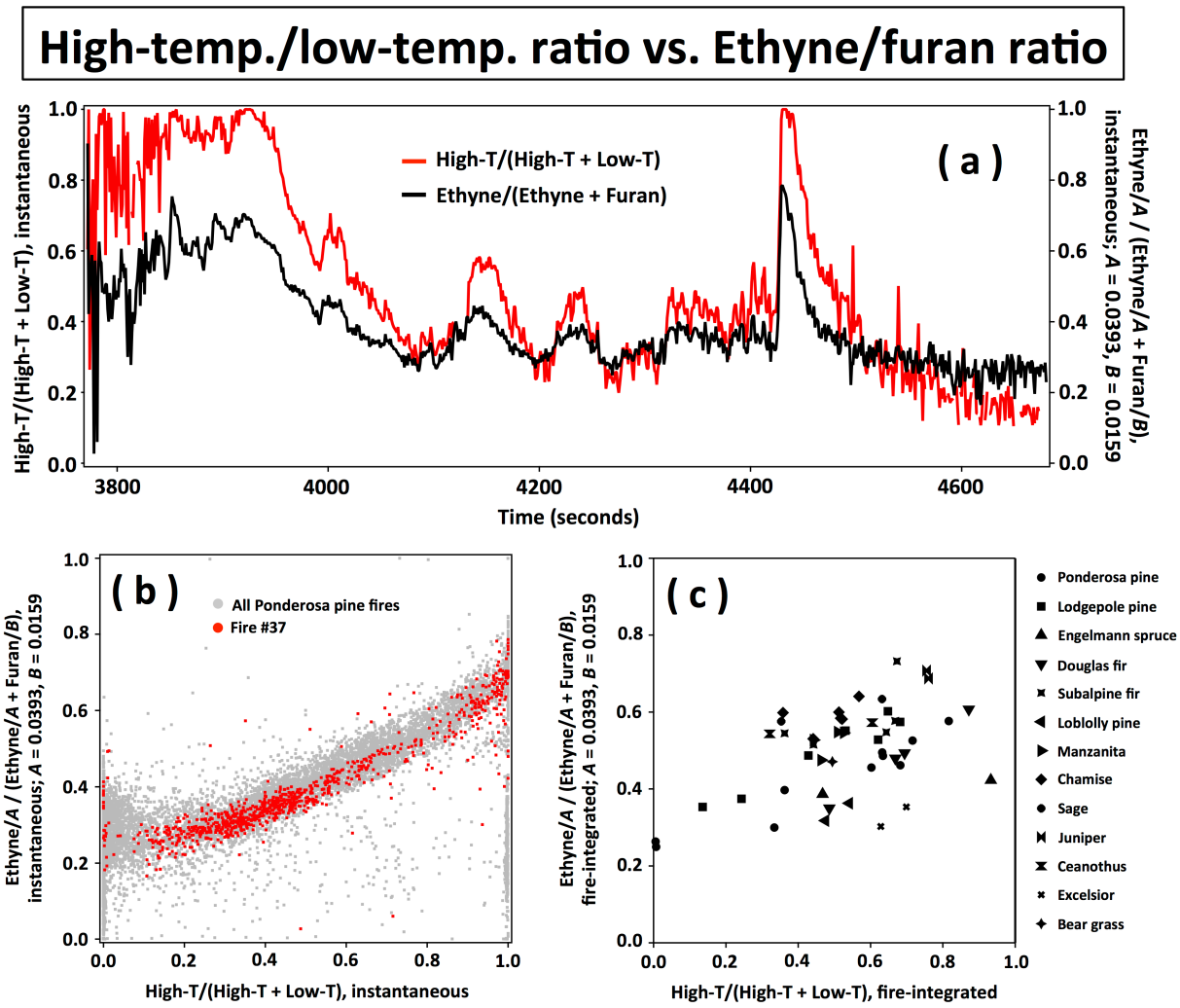

Figure S9. The comparison of contribution of high-temperature factor versus ethyne/furan ratio. (a) Time series of Fire #37 (Ponderosa pine realistic mixture). (b) Scatter plot of instantaneous high-temperature contribution versus ethyne/furan ratio for all Ponderosa pine fires. (c) Scatter plot of fire-integrated high-temperature contribution versus ethyne/furan ratio for all fires. Contribution of high-temperature factor was calculated by $\Sigma VOC_{high\text{-}T}/(\Sigma VOC_{high\text{-}T} + \Sigma VOC_{low\text{-}T})$ instantaneously or on a fire-integrated basis. Ethyne/furan ratio was calculated by $\frac{Ethyne/A}{Ethyne/A + Furan/B}$ instantaneously or on a fire-integrated basis. Coefficients *A* and *B* correspond to 0.0393 (in ppbv/total VOC ppbv) for ethyne in the high-temperature factor and 0.0159 (in ppbv/total VOC ppbv) for furan in the low-temperature factor, respectively.

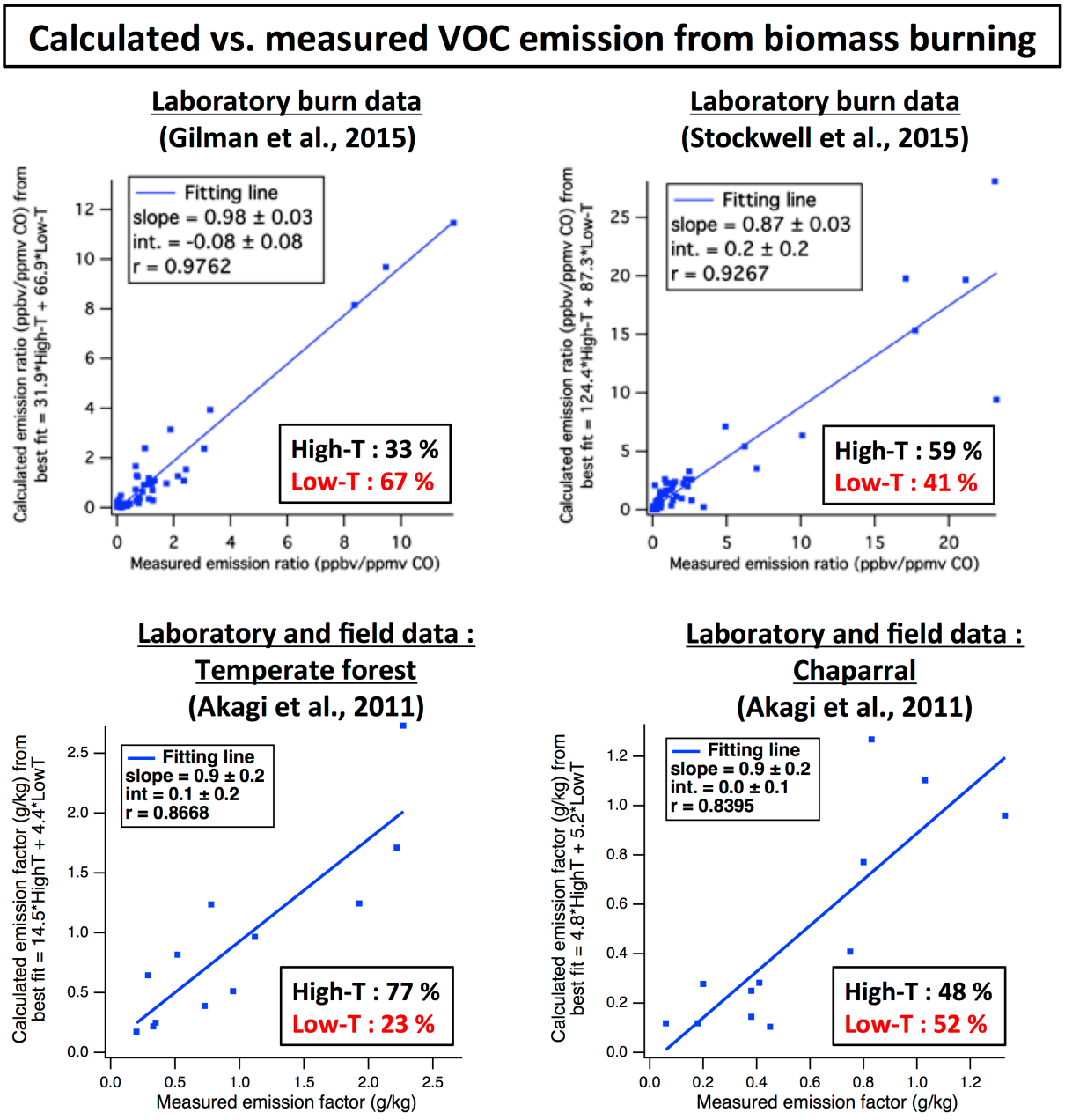

Figure S10. Scatter plots of calculated versus measured emissions for three literature data. Calculate emissions were obtained by fitting the VOC emission profiles (Figure 3). Laboratory study reported by Gilman et al. (2015) used fuels from southwestern, southeastern, and northern U.S. (e.g., pine, spruce, fir, chaparral, mesquite, and oak), while in the case of Stockwell et al. (2015), several types of grass, spruce, and chaparral were used.

S1. Preparation of datasets for PMF analysis

S1.1. Ion signal datasets

Ion signal datasets for PMF analysis were prepared using five steps. (i) 2 Hz time series data were averaged to 1 Hz. (ii) Background was subtracted from each ion signal before application of PMF, to avoid having PMF return a factor that describes the background. Background was determined from a 30-second to 5-minute measurement of combustion chamber air immediately prior to the fire. (iii) Points where instrument signal was negative or less than 0.01 were replaced with 0.01, which is based on the lowest limit of ion signal (ncps) of the PTR-ToF-MS. (iv) Data were restricted to the time period of active fire emissions, defined by the first enhancement of benzene above background (start) to when the PTR-ToF-CIMS stopped sampling (end). (v) The resulting time series for all fires of a particular fuel type (e.g., Ponderosa pine) were concatenated into a single data matrix.

S1.2. Uncertainty datasets

PMF also requires an estimate of measurement uncertainty of ion signals at each time point for each ion mass (*m/z*). The uncertainties ($\sigma_{m/z}$) were estimated as $\sigma_{m/z}\,(ncps) = 2.0 \times \sqrt{N_{m/z,w/o\ BG}\,(ncps)}$, where $N_{m/z,\ \mathrm{w/o\ BG}}$ is background-subtracted ion signal. The derivation is described below.

The uncertainty used in the present work is in units of "normalized counts-per-second (ncps)". The ncps uncertainty should have the same value relative to the ncps signal, as the uncertainty of the raw ion signal in units of counts-per-second (cps) relative to the cps signal. The raw ion signal (cps) is without normalization by the H_3O^+ ion intensities and correction for the ToF-duty cycle. The present uncertainty value ($\sigma_{m/z}$) for a given *m/z* ion signal ($N_{m/z}$) can be calculated as follows:

$$\sigma_{m/z}\,(ncps) = A \times \sqrt{N_{m/z}\,(ncps)} \times t \tag{S1-a}$$

$$A = \alpha_{m/z} \times \sqrt{\frac{10^6}{I_{H3O+}\,(cps)}} \times \sqrt{\frac{m/z_{reference}}{m/z}} \tag{S1-b}$$

A is a scaling factor of $\sqrt{N_{m/z}}$. $\alpha_{m/z}$ is a coefficient relative to the Poisson (counting) statistics ($\sigma = \sqrt{N}$) that accounts for additional noise to the ion signals of the masses due to the high-resolution peak fitting of the ToF mass spectra (Cubison et al., 2015; Corbin et al., 2015; Yuan et al., 2016). I_{H3O+} is the raw intensity of the H_3O^+ reagent ion, $m/z_{reference}$ is an arbitrary reference mass (in this work, $m/z_{reference}$ = 55), and t the sampling time (in this case, t = 1 s). The factors $10^6/I_{H3O+}$ and $\sqrt{m/z_{reference}/m/z}$ are to undo normalization by the H_3O^+ ion intensities and correction for the ToF-duty cycle, respectively.

Here we estimated a scaling factor $\alpha_{m/z}$ in Eq. (S1) suitable for the present instrumentation. Figure S1.1 shows standard deviations of the background signals (in units of cps) versus the background signals themselves from the individual zeroing periods for the 574 ion species listed in Table S2 during one burn (Fire #02). Most of data points are observed in the region between $\sqrt{N}$ and $3 \times \sqrt{N}$, suggesting that high-resolution peak fitting in this work can increase the errors in the ion signals by as much as a factor of 3 for the ion peaks. Figure S1.2 shows the empirically determined coefficient $\alpha_{m/z}$ (i.e., the ratio of standard deviation to $\sqrt{N}$) and scaling factor A (Eq. S1-b) for each m/z ion. It is seen that both the factors can be approximated as a constant (1.2 ± 0.4 and 0.6 ± 0.2, respectively), across a wide range of m/z. Accordingly, the empirical determined scaling factor A in Eq. (S1) can be approximated as 0.6, independent of the m/z value.

Based on the results described above, we first performed PMF using datasets of ion signals with backgrounds and uncertainties calculated from the empirical determined scaling factor A = 0.6 for single burn data (Fire #02, Ponderosa pine realistic mixture). The resulting 3-factor solution returned the high-temperature and low-temperature pyrolysis mass spectral and time series profiles as well as background profiles, but Q/Q_{exp} value was quite high (9.69 with fPeak and seed of zero). "Q" is a fit parameter of the PMF algorithm and is expressed by summation of squared scaled residuals for each experimental data points, i.e., $Q = \Sigma(\text{Resid}/\sigma)^2$ (Paatero, 1997; Ulbrich et al., 2009). Scaled residual (Resid/σ) at a certain data point is calculated as the ratio of residual (Resid) not fit by the PMF to uncertainty (σ) at that point. "Q_{exp}", expected Q, is associated with abs Resid/$\sigma \sim 1$. The value of $Q/Q_{exp} >> 1$ indicates underestimation of the uncertainties (Ulbrich et al., 2009). Thus, we performed several tests to see how sensitive the PMF results are to the uncertainty estimate, by setting A = 1.0, 1.5, 2.0, 2.5, and 3.0 and applying PMF. The profiles of the 3-factor solutions for individual uncertainty datasets were nearly

identical to the case of A = 0.6 (correlation coefficient > 0.99 as shown in Figure S1.3). Some small differences were seen in the quality of fit for ions with average enhancements of less than 10 ncps (corresponding to approximately 130 pptv and << 1% of total signal). These differences do not affect any of our conclusions. Interestingly, the Q/Q_{exp} value decreased with increasing the number of A: Q/Q_{exp} = 4.95, 2.65, 1.64, 1.12, and 0.78 for A = 1.0, 1.5, 2.0, 2.5, and 3.0, respectively (fPeak = seeds = 0, discussed in next section). Taking into account the Q/Q_{exp} value and the quality of fit, we decided A = 2.0 as the best number here.

Furthermore, we investigated changes to the PMF solution when using (i) the background-subtracted ion signals and (ii) concatenated burn data. If backgrounds are subtracted, or burns concatenated, the PMF results are quite similar to the base case obtained from the ion signals with backgrounds, A = 0.6, and single burn data (correlation coefficient r > 0.97 as shown in Figure S1.4). Consequently, the uncertainty datasets for concatenated burn data were prepared $\sigma_{m/z}\ (ncps) = 2.0 \times \sqrt{N_{m/z,w/o\ BG}\ (ncps)}$.

S1.3. Effect of rotational ambiguity (fPeak) and starting points (seeds) on PMF results

A subset of the rotational freedom of the 2-factor PMF solutions was explored by varying the fPeak values from -1.0 to +1.0, for the concatenated burn datasets consisting of the background-subtracted ion signals $N_{m/z,w/o\ BG}$ (ncps), and the uncertainty $\sigma_{m/z}\ (ncps) = 2.0 \times \sqrt{N_{m/z,w/o\ BG}\ (ncps)}$. In this study, solutions obtained from nonzero fPeak values (fPeak ≠ 0) were generally consistent with those from zero fPeak value (fPeak = 0). The resulting Q/Q_{exp} are almost constant (3.0292 ± 0.0003, as shown in Figure S1.5a). This means that the results shown in this work are associated to no rotation in the PMF analysis. In contrast, different random starting points (seeds = 0 – 10) were tried to find the local minimum of Q/Q_{exp} in the 2-factor PMF solutions (Paatero, 1997). The local minimum was obtained at seeds = 0 (Figure S1.5b). Therefore, the discussion in Section 3 in the main text is based on the 2-factor PMF solutions at fPeak = seeds = 0.

S2. Relationship of ethyne:furan ratio to high:low temperature ratio

Trace gases can be used to estimate the emissions from the high-/low-temperature factors. Here we propose ethyne (C_2H_2) and furan (C_4H_4O) as tracers. Normalized fractions of the high-/low-temperature factors are 72%/28% for ethyne and 33%/67% for furan. These two

compounds have large emissions and low standard deviations in the average emission profiles of 15 different fuels (0.0393 ± 23% ppbv/total VOC ppbv for ethyne in the high-temperature factor and 0.0159 ± 19% ppbv/total VOC ppbv for furan in the low-temperature factor). This reduces to a ratio of approximately:

$$\frac{total\ VOC\ ,high\ temperature\ (ppbv)}{total\ VOC\ ,low\ temperature\ (ppbv)} = \frac{ethyne\ (ppbv)/0.0393}{furan\ (ppbv)/0.0159} \quad \text{(S2)}$$

Average relative error (%) of the ethyne/furan ratio to the total $VOC_{High\text{-}T}$/total $VOC_{Low\text{-}T}$ is 50%, except for rotten wood.

References

Cubison, M. J., and Jimenez, J. L.: Statistical precision of the intensities retrieved from constrained fitting of overlapping peaks in high-resolution mass spectra, Atmos. Meas. Tech., 8, 2333-2345, https://doi.org/10.5194/amt-8-2333-2015, 2015.

Corbin, J., Othman, A., Allan, D. J., Worsnop, R. D., Haskins, D. J., Sierau, B., Lohmann, U., and Mensah, A. A.: Peak-fitting and integration imprecision in the Aerodyne aerosol mass spectrometer: effects of mass accuracy on location- constrained fits, Atmos. Meas. Tech., 8, 4615-4636, https://doi.org/10.5194/amt-8-4615-2015, 2015.

Paatero, P.: Least squares formulation of robust non-negative factor analysis, Chemometr. Intell. Lab., 37 (1), 23-35, https://doi.org/10.1016/S0169-7439(96)00044-5, 1997.

Ulbrich, I. M., Canagaratna, M. R., Zhang, Q., Worsnop, D. R., and Jimenez, J. L.: Interpretation of organic components from Positive Matrix Factorization of aerosol mass spectrometric data, Amos. Chem. Phys., 9 (9), 2891-2918, http://doi.org/10.5194/acp-9-2891-2009, 2009.

Yuan, B., Koss, A., Warneke, C., Gilman, J. B., Lerner, B. M., Stark, H., and de Gouw, J. A.: A high resolution time-of-flight chemical ionization mass spectrometer utilizing hydronium ions (H_3O^+ ToF-CIMS) for measurements of volatile organic compounds in the atmosphere, Atmos. Meas. Tech., 9 (6), 2735-2752, http://doi.org/10.5194/amt-9-2735-2016, 2016.

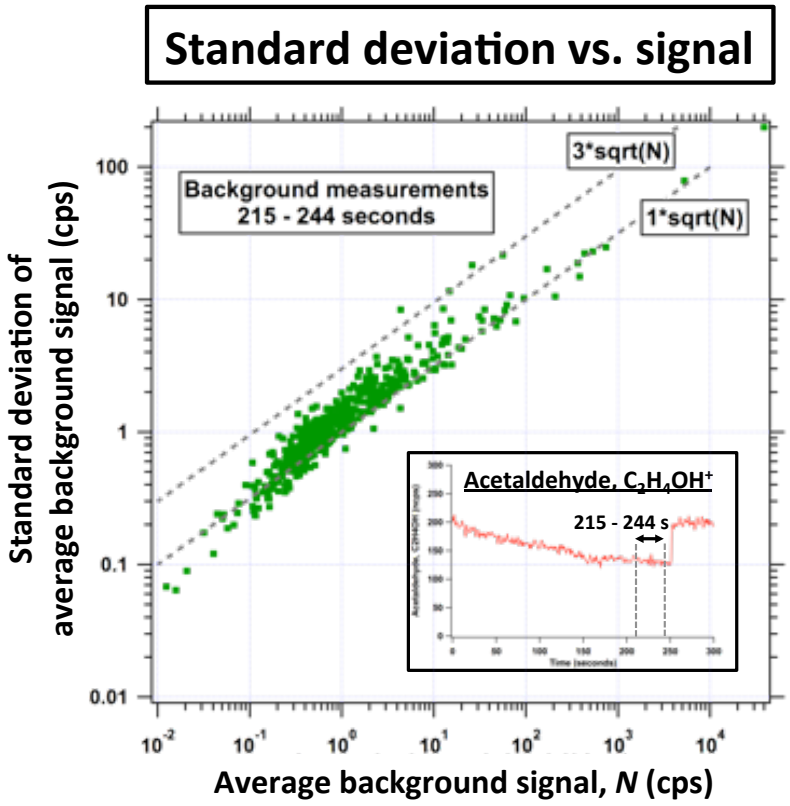

Figure S1.1. Scatterplot of the standard deviations of background signals versus the measured background signals from Fire #02 for 574 ion peaks which were used for PMF analysis. In this graph, the signals are not corrected for the H_3O^+ ion intensities and the ToF duty cycle. The two dashed lines are $\sqrt{N}$ and $3 \times \sqrt{N}$, respectively.

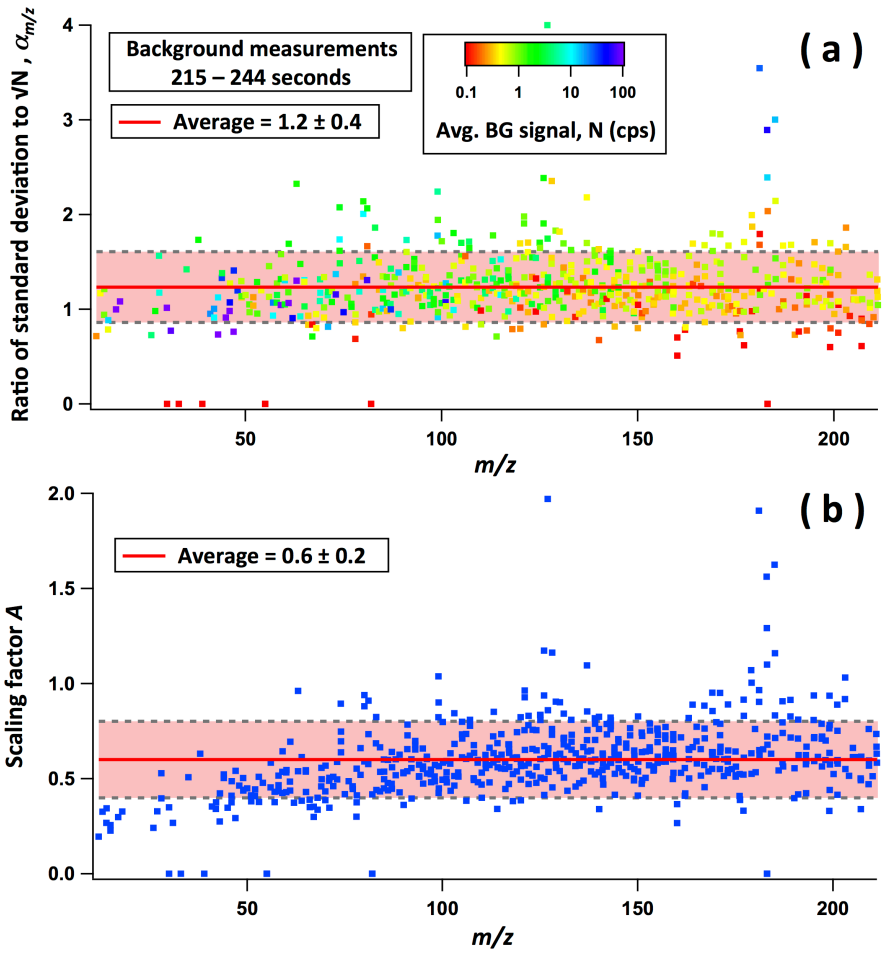

Figure S1.2. Scatterplots of (a) ratio of standard deviation to background signals ($\alpha_{m/z}$) and (b) scaling factor A versus the m/z values. The coefficient $\alpha_{m/z}$ was obtained from the data shown in Figure S1.1. The scaling factor A was determined from Eq. S1-b and the average $\alpha_{m/z}$ value of 1.2.

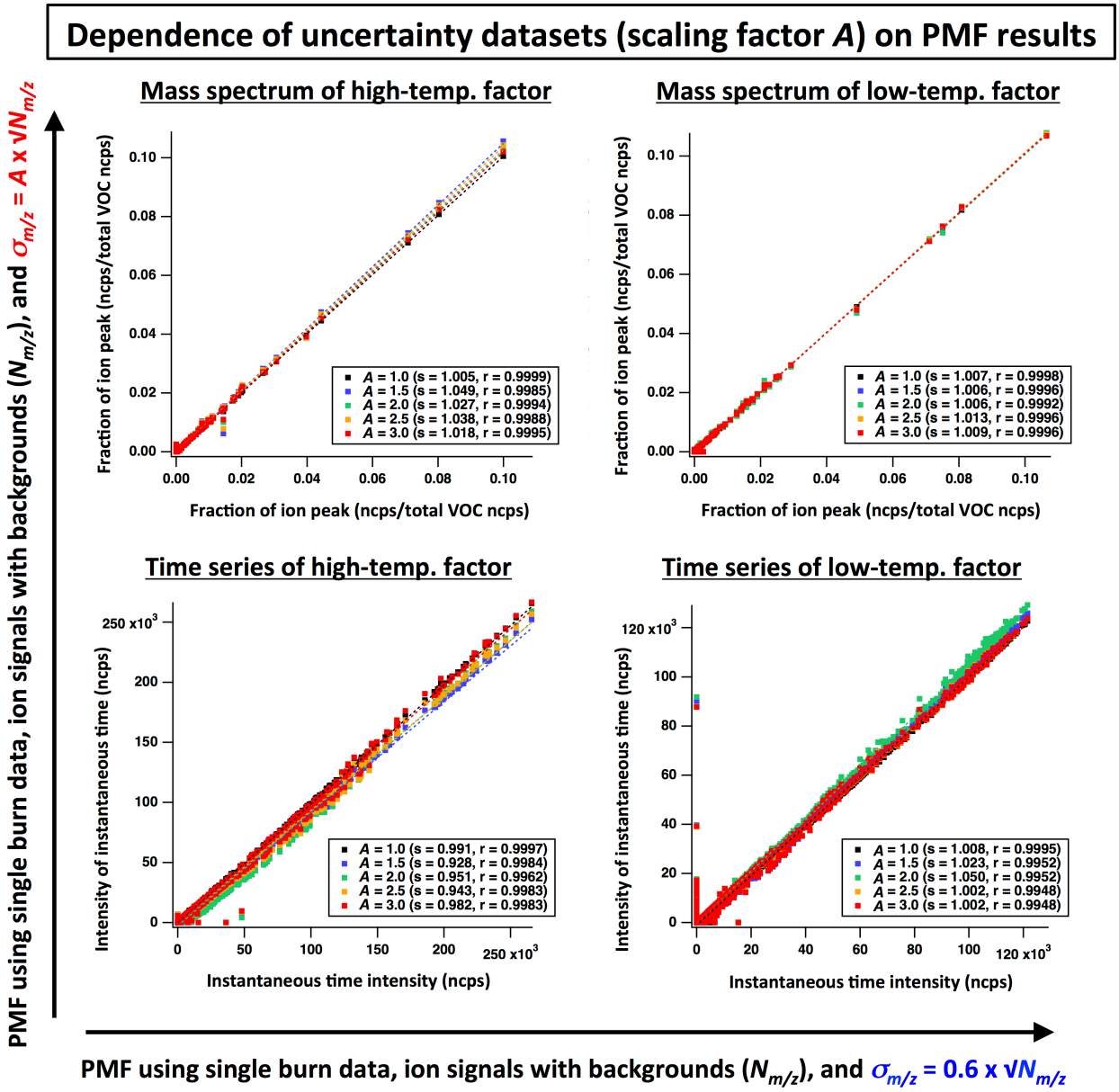

Figure S1.3. Dependence of uncertainty datasets, scaling factor *A* in Eq. (S1), on PMF results (mass spectra and time series for high- and low-temperature pyrolysis factors at fPeak = seeds = 0). The PMF results obtained from scaling factor *A* = 1.0, 1.5, 2.0, 2.5, and 3.0 are compared with the results from *A* = 0.6. Single fire data (Fire #02, Ponderosa pine realistic mixture) and ion signals with backgrounds are used. "s" and "r" in each panel represent the slope and correlation coefficient for the linear line of the best fit, respectively.

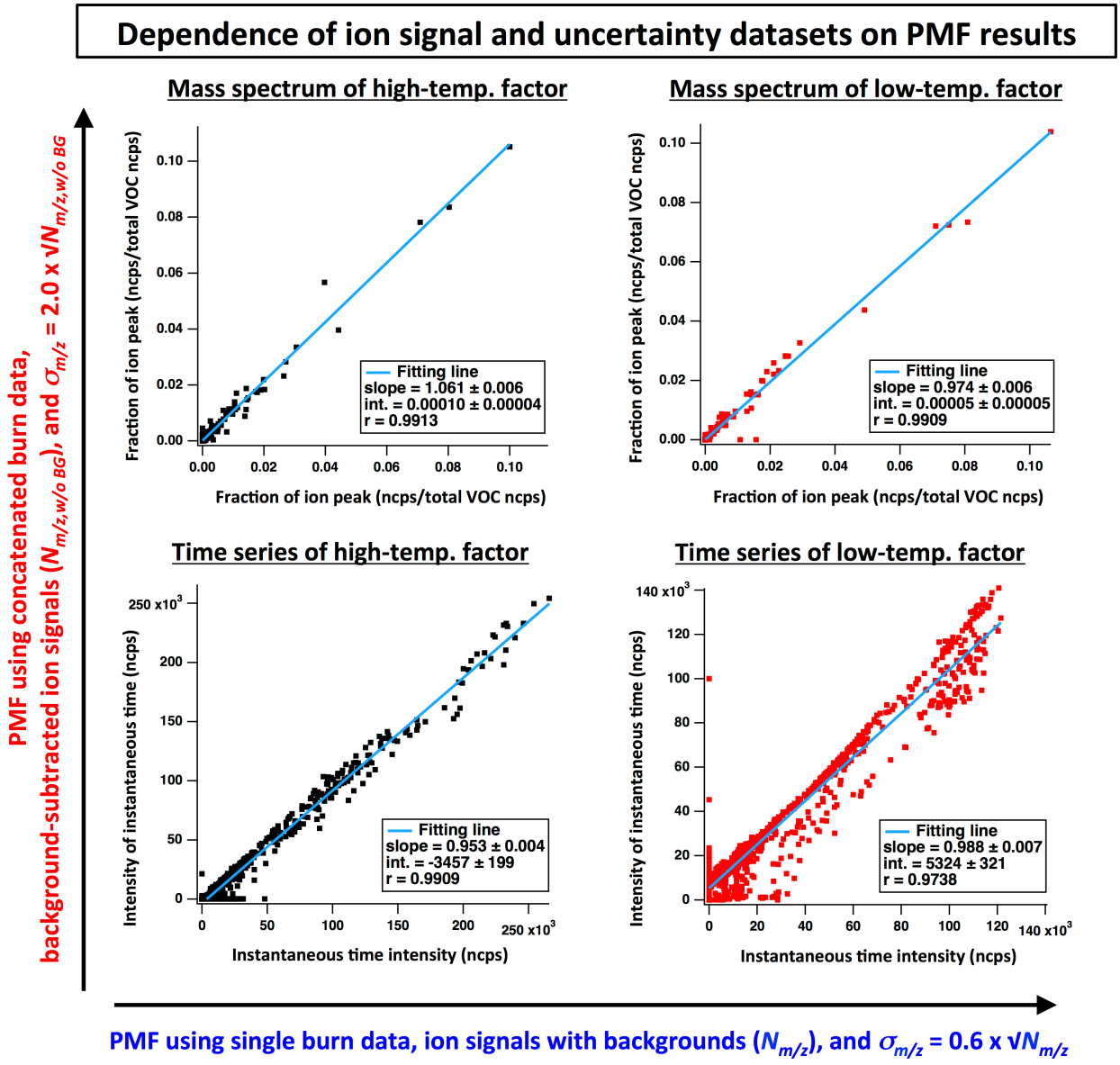

Figure S1.4. Dependence of ion signal and uncertainty datasets on PMF results (mass spectra and time series for high- and low-temperature pyrolysis factors at fPeak = seeds = 0). The PMF results obtained from concatenated burn data (10 Ponderosa pine burn data), background-subtracted ion signals, and the scaling factor A = 2.0 in Eq. (S1) are compared with the results from single burn data (Fire #02, Ponderosa pine realistic mixture), ion signals with backgrounds, and A = 0.6.

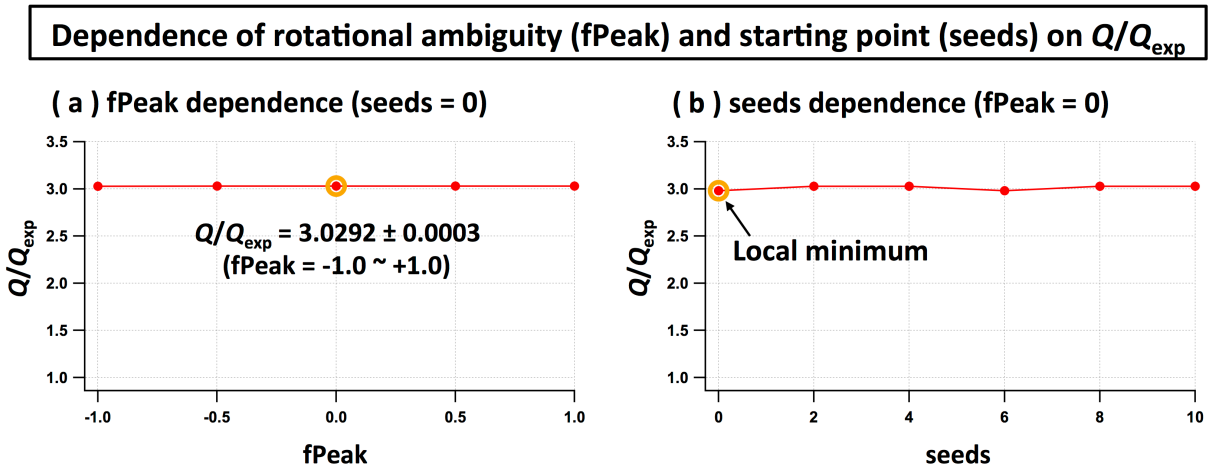

Figure S1.5. Dependence of rotational ambiguity (fPeak) and starting point (seeds) on Q/Q_{exp} for the 2-factor PMF solutions of the concatenated Ponderosa pine burn datasets. These datasets consist of the background-subtracted ion signals $N_{m/z,w/o\ BG}$ (ncps), and the uncertainty $\sigma_{m/z}\ (ncps) = 2.0 \times \sqrt{N_{m/z,w/o\ BG}\ (ncps)}$.